COBEM 2023 27TH INTERNATIONAL CONGRESS OF MECHANICAL ENGENEERING

ABCM Brazilian Society of Mechanical Sciences and Engineering
27th ABCM International Congress of Mechanical Engineering
December 04-08, 2023, Florianópolis-SC, Brazil

COB-2023-1287
WAKE INTERACTION BETWEEN TWO CIRCULAR SLENDER CYLINDERS TANDEM PLACED WITH SMALL SPACING RATIOS

Patrick Batista Habowski
Adriane Prisco Petry
Universidade Federal do Rio Grande do Sul, Programa de Pós-Graduação em Engenharia Mecânica (PROMEC), Rua Sarmento Leite, 425, Porto Alegre, CEP 90050-170, Brazil.
patrick.habowski@ufrgs.br
adrianep@mecanica.ufrgs.br

Sérgio Viçosa Möller
Universidade Federal do Rio Grande do Sul, Programa de Pós-Graduação em Engenharia Mecânica (PROMEC), Rua Sarmento Leite, 425, Porto Alegre, CEP 90050-170, Brazil.
svmoller@ufrgs.br

Abstract. *The present article is an experimental investigation of two circular cylinders tandem assembled inside a wind tunnel. The cylinder setup is free to oscillate in the lateral direction and was mounted distancing the cylinder's centers by a longitudinal distance L. Three L/D spacing ratios varying the imposed flow velocity were tested, where D is the cylinder diameter, generating Reynolds numbers in the range of 9.6 to 16.6 × 10³. To study the wake interaction between the cylinders, the lateral acceleration was measured by two accelerometers positioned inside both cylinders. In addition, two hot-wire anemometers were assembled behind the downstream cylinder to monitor the wake velocity in the bottom and middle height of the downstream cylinder. Post-processed results of the acquired signals were performed by Matlab software using Fourier and wavelet analysis. The main results presented the highest levels of oscillation for the configuration with the smaller proposed L/D spacing ratio of 3. High fluctuation values were observed in the wake flow velocity results of the anemometer located at the middle height of the downstream cylinder due to the lateral oscillation. The predominant frequency observed in the lateral movement was 2.4 Hz. Strouhal numbers identified the vortex shedding of the downstream cylinder.*

Keywords: *Circular Cylinders, Energy Harvesting, Statistical Analysis, Turbulent Flow, Wind Tunnel.*

1. INTRODUCTION

The cross-flow on arrangements with circular cylinders was very explored through the last decades, where studies discussing force coefficients, Strouhal numbers, flow visualization, energy content analysis, and others, were reported in the literature (Igarashi, 1981, Païdoussis, 1982, Zhou and Alam, 2016). Engineering applications with circular cylinder structures can be simple, as in the case of chimneys, transmission lines, and bridge structures, but also more complex, like tube banks and heat exchangers in nuclear reactors. Vibrational regimes are reported in such structures depending on how these cylinders are positioned to the flow (Alam et al., 2003a, 2003b). This phenomenon occurs because the vortex shedding from the upstream cylinder modifies the pressure field of the downstream cylinder. The intensity of these vibrational regimes is a very important topic of study since they can lead to structural damage (Chen, 1985, 1987). On the other hand, whether such vibrational regimes can be controlled, this energy can be converted into useful energy on small scales, the so-called energy harvesting (Pryia, 2007, Scarselli et al., 2016).

As an effort to summarize the main studies about the flow on circular cylinders of the past decades, literature reviews were presented by authors such as Païdoussis (1982), Sumner (2010), and Zhou and Alam (2016). These authors presented literature reviews for cylinder studies with several configurations of flow regime, varied numeric approaches, experiments in hydrodynamic and wind tunnels, several configurations for the number and shape of the cylinders, and so forth. In each study, the authors diagrammed the main results of force coefficients, Strouhal numbers, heat transfer coefficients, wake flow patterns, and flow visualization, for a huge number of experiments previously performed by themselves and by other relevant authors.

Two circular cylinders in tandem arrangement submitted to a turbulent crossflow is a particular application among the several configurations observed in the study of flow over cylinders. In such configuration, the upstream cylinder is positioned in front of the downstream cylinder, separated by an axial distance $\boldsymbol{L}$. Thus, the wake from the upstream cylinder affects the behavior of the second cylinder, where two main flow mechanisms are reported: Vortex-Induced Vibration (VIV) and Wake-Induced Vibration (WIV). Both flow mechanisms are strongly dependent on the spacing ratio $\boldsymbol{L/D}$, where $\boldsymbol{D}$ is the cylinder diameter.

The response of a typical WIV, observed in high spacing ratios, is marked by a continuous increase in amplitude even at high reduced velocities. This sets it apart from a VIV response, which occurs within a limited range of resonance. In the case of WIV, the downstream cylinder is affected by the vortex street generated by the wake of the upstream flow. The phase lag between displacement and fluid force enables the transfer of energy from the flow to the structure, thereby maintaining the oscillations (Assi et al., 2010). Park et al. (2018) presented experimental results on WIV and VIV acting on two circular cylinders. The study performed scenarios where the upstream cylinder was either fixed or allowed one degree of freedom motion, while the downstream cylinder was assembled with two degrees of freedom. The spacing ratio $\boldsymbol{L/D}$ ranged from 3.0 to 10. In the tandem configuration, both WIV and VIV responses were observed. The impact of WIV was most pronounced at $\boldsymbol{L/D}$ values of 3.0 and 4.0.

Derakhshandeh et al. (2014) conducted a numerical VIV analysis of the flow around two circular cylinders, considering both tandem and staggered configurations. Their study revealed a direct correlation between the arrangement of the two cylinders and the amount of kinetic energy that can be harnessed through VIV. The optimal tandem arrangement for achieving maximum vibration response occurred when the downstream cylinder was positioned within the range of $3.5 \leq \boldsymbol{L/D} \leq 4.5$.

In the study proposed by Igarashi (1981), six distinct flow patterns were identified for configurations where circular cylinders were tandem placed. These patterns are primarily influenced by the Reynolds number and the spacing ratio $\boldsymbol{L/D}$ between the cylinders. Similarly, Alam et al. (2003b) conducted a study focusing on tandem circular cylinders at a subcritical Reynolds number and examined various $\boldsymbol{L/D}$ spacing ratios. The study systematically analyzed the results concerning drag, lift, and pressure coefficients, their fluctuations, reattachment positions of shear layers, and Strouhal numbers. The main conclusions emphasized the high sensitivity of fluctuating drag and lift forces to the $\boldsymbol{L/D}$ spacing ratio, along with their influence on the reattachment of shear layers in the downstream cylinder.

The control of vortex shedding holds significant importance in aeroacoustics applications due to its potential implications. Noufal et al. (2022) conducted an experimental study using a control rod to manage the vortex shedding of a single circular cylinder. The control rod was tested at various angular positions in proximity to the cylinder. The results demonstrated that the control rod had an impact on the Strouhal numbers, allowing an increase or decrease in the frequency of vortex shedding and the associated acoustic pressure peak, depending on its relative angular position to the cylinder.

In our laboratory, several studies were carried out exploring the flow over circular cylinders placed side-by-side in fixed and free-to-oscillate/rotate configurations, tandem placed with oscillatory regime, and tube banks with several arrangements. Varela et al. (2017) examined the bistability phenomenon of wake patterns in side-by-side circular cylinders. The experimental setup involved placing the cylinders on a circular table that was set as free to rotate. When subjected to turbulent flow, the setup initially exhibited oscillations, which persisted and intensified after a few seconds. This phenomenon was further investigated by Habowski et al. (2020a), who conducted flow visualization experiments in a hydraulic channel using a pair of fixed circular cylinders. The study focused on describing the wakes formed downstream of the cylinders and their interactions at different angles between the cylinder setup and the flow.

Neumeister et al. (2021) performed experiments to investigate the Fluid-Induced Vibration (FIV) interaction of single cylinders and pairs of cylinders arranged in tandem and side-by-side configurations. The study involved 25 experiments with variations in the damping $\boldsymbol{\zeta}$ and mass ratios $\boldsymbol{m^*}$ of the cylinders. Notably, a sudden increase in the amplitude of transversal oscillations was observed when both cylinders were allowed to vibrate freely. Building upon the experiments conducted by Neumeister et al. (2021), Habowski et al. (2020b) performed a separate experiment with two circular cylinders assembled on a circular table, which was set as free to rotate, inside a wind tunnel. The upstream cylinder was aligned with the centerline of the circular table, while the downstream cylinder was eccentrically positioned. Throat-like devices were introduced near the cylinders to enhance flow acceleration and induce oscillations in the cylinder setup, even at low free-flow velocities. The authors reported a proportional relationship between the Reynolds number and the amplitude of the oscillations.

More recently, Habowski et al. (2022) presented a numerical study of two slender circular cylinders tandem placed and fixed inside a channel, considering spacing ratios $\boldsymbol{L/D}$ of 5, 7.5, and 10. The authors proposed LES simulations identifying the force coefficients, Strouhal numbers, axial velocity discussion, and flow visualization. Results presented good accordance with experimental observations performed by Neumeister et al. (2022), and also with the results presented by Alam et al. (2003b) and Alam and Meyer (2011). The main conclusions pointed out the higher influence of the upstream vortex shedding on the downstream cylinder fluid forces for the lowest tested spacing ratio $\boldsymbol{L/D}$ of 5. Increasing the spacing ratio $\boldsymbol{L/D}$ to 10, the effects of vortex shedding from the upstream cylinder are still present, but with lower impact.

Considering the above discussion, this work intends to present experimental results using two circular tandem slender cylinders with one degree of freedom, where the cylinders are free to oscillate in the transversal direction of the flow. The pair of cylinders was assembled inside a wind tunnel, and the lateral acceleration and the wake flow velocity were measured. Free flow velocities from 5.7 to 10 m/s were imposed, generating Reynolds numbers from 9.5×10^3 to 16.6×10^3, considering the cylinder diameter $\boldsymbol{D}$. Spacing ratios $\boldsymbol{L/D}$ of 3, 4, and 5 were tested. The obtained results were post-processed using statistical mathematical tools such as Fourier and wavelet analysis by the Matlab software.

2. MATHEMATICAL BACKGROUND

Statistical analysis can be carried out considering time, frequency, and time-frequency domains. An initial and very useful time domain statistical approach in the study of turbulent flows is presented by Tennekes and Lumley (1972) as the four statistical moments. Computing the four statistical moments consists of calculating the temporal mean value, the standard deviation, the skewness, and the kurtosis of a time series (Eqs. 1–4, respectively). The standard deviation can be understood as the mean fluctuations of such time series. The skewness is directly linked to the asymmetry of the signal, being zero for a time series perfectly symmetric. Lastly, kurtosis is related to the flatness of the time series, being high if there are tails in the signal.

$$\bar{u} = \frac{\sum u}{n} \tag{1}$$

$$\sigma^2 = \overline{u'^2} \tag{2}$$

$$S_k = \frac{\overline{u'^3}}{\sigma^3} \tag{3}$$

$$K = \frac{\overline{u'^4}}{\sigma^4} \tag{4}$$

In Equations (1–4), $\bar{\boldsymbol{u}}$ is the mean temporal value of the instantaneous velocity $\boldsymbol{u}$, $\boldsymbol{n}$ is the number of samples in the time series, $\boldsymbol{\sigma^2}$ is the standard deviation, $\boldsymbol{S_k}$ and $\boldsymbol{K}$ are the dimensionless values of skewness and kurtosis, respectively. The value $\boldsymbol{u'}$ is the velocity fluctuation and is defined as the difference between the instantaneous velocity and the mean temporal value, $\boldsymbol{u' = u - \bar{u}}$.

The frequency-domain analysis can be performed using the Fourier analysis, but through this mathematical tool is not possible the identification of non-stationary phenomena. The non-stationary phenomena observed in the present study demanded wavelet analysis which allows the time-frequency window analysis (Indrusiak and Möller, 2011, Indrusiak et al., 2016, Percival and Walden, 2000). While the Fourier transform uses trigonometric functions as the basis, the basis of wavelet transforms are functions called wavelets with finite energy and zero average. Thus, it is possible to stretch and compress the window of the windowed Fourier transform, and only the scales of interest in time and frequency domains are reported. The continuous wavelet transform (CWT) of an arbitrary function $\boldsymbol{x(t)}$ is given by Eq. (5). The wavelet spectrum, called spectrogram, is defined by Eq. (6), where the energy is related to each time and scale or frequency. This characteristic allows the representation of the energy of this transient signal over time and frequency domains.

$$\tilde{X}(a,b) = \int_{-\infty}^{+\infty} x(t)\psi_{a,b}(t)\,dt \quad a,b \in \Re \tag{5}$$

$$P_{xx}(a,b) = \left|\tilde{X}_{a,b}\right|^2 \tag{6}$$

In Equations (5–6), $\boldsymbol{\tilde{X}(a,b)}$ is the generic function in the wavelet domain, $\boldsymbol{a}$ and $\boldsymbol{b}$ are wavelet parameters, $\boldsymbol{\psi_{a,b}(t)}$ is a generic wavelet function, and $\boldsymbol{P_{xx}(a,b)}$ is the spectrogram of $\boldsymbol{\tilde{X}(a,b)}$. In the present work, the wavelet analysis was also used to determine the Discrete Wavelet Transform (DWT), which decomposes the signal in dyadic frequency ranges. The DWT (Eq. 7) decomposes the energy of the time series in the respective scales and the summation of Eq. (7) can be considered as a portion of energy due to the fluctuations in $\boldsymbol{2^{j-1}}$ scale. When a time series is described by a DWT with more than $\boldsymbol{2^j}$ elements it is used the Eq. (8) for $\boldsymbol{1 \leq j \leq J}$, where $\boldsymbol{J}$ is a reasonable choice based on the frequency scales of interest.

$$\tilde{X}(j,k) = \sum_t x(t)\,\psi_{j,k}(t) \quad j,k \in \Re \tag{7}$$

$$\tilde{X}(J,k) = \sum_t x(t)\,\phi_{J,k}(t) \tag{8}$$

In Equations (7–8), $\widetilde{\boldsymbol{X}}(\boldsymbol{j},\boldsymbol{k})$ is the wavelet series for the given $\boldsymbol{j}$ and $\boldsymbol{k}$ coefficients, $\boldsymbol{j}$ is the dilatation coefficient, $\boldsymbol{k}$ is the translation coefficient, and $\boldsymbol{\phi_{J,k}(t)}$ is the scaling function associated with the wavelet function. A time series and its discrete wavelet transform are both mathematical representations of a physical phenomenon. Thus, for a given sampling frequency $\boldsymbol{F_s}$, any discrete time series can be represented by Eq. (9).

$$x(t) = \sum_{k} \tilde{X}(J,k)\phi_{J,k}(t) + \sum_{J\leq 1}\sum_{k} \tilde{X}(j,k)\phi_{J,k}(t) \tag{9}$$

The first term of Eq. (9) is the approximation of the signal at the scale $\boldsymbol{J}$, and the second term is the details of the signal at the scales $\boldsymbol{j}$. The wavelet analysis employed in this work is a Db20 function with reconstruction level 6. Thus, considering the sampling frequency and the reconstruction level, the reconstructed signals were generated with spectral components ranging from 0 to 7.8125 Hz according to Eq. (10).

$$Frequency\ Interval = [0, Fs/\ 2^{J+1}] \tag{10}$$

3. EXPERIMENTAL METHODOLOGY

The experimental study was performed in a wind channel of the Laboratory of Fluid Mechanics, located at the Federal University of Rio Grande do Sul (LMF). The wind channel is a rectangular square sized with 1000 mm of edge and 7000 mm long. The air from the surroundings is used as the working fluid, which is sucked by an axial blower into the wind channel (Fig. 1, detail F). This air is accelerated by a nozzle (Fig. 1, detail A) and passes by a protective screen and a honeycomb (Fig. 1, details B and C, respectively) to homogenize the flow. Then, the airflow achieves the test section (Fig. 1, detail D), where the setup with the cylinders is assembled. After passing the cylinder's setup, the airflow passes through a convergence section (Fig. 1, detail E) and the axial blower (Fig. 1, detail F), finally returning to the environment. A frequency inverter (Fig. 1, detail G) is used to control the rotational velocity of the axial blower. The channel walls are made of wood panels, and an external structure of iron is used to ensure the hardness of the wind channel. One of the sidewalls in the test section (Fig. 1, detail D) is made of acrylic glass to allow the visualization of the experiment. A pitot tube is also positioned in this region to measure the free flow velocity.

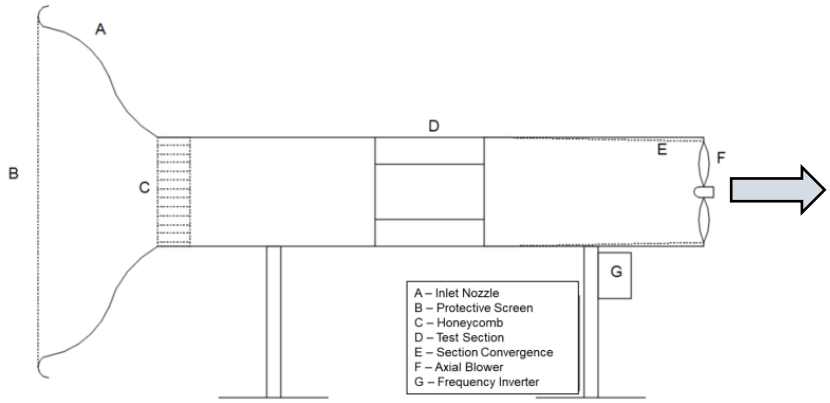

Figure 1 – Schematic view of the wind tunnel. Flow from left to right.

Two circular cylinders with 25 mm in diameter and 800 mm long were used in the present study, leading to an aspect ratio of 32. The construction material of both cylinders is carbon fiber, chosen because of its smoothness and low specific mass. This set of cylinders was assembled on an acrylic glass table, transversally mounted inside the wind tunnel, as presented in Fig. 2a. The table is fixed 200 mm from the top wall. Each cylinder is fixed on a rigid 3D-printed support (coupling), which allows the correction of small misalignments in the assembly. In each of these supports, two low-wear bearings are inserted, connecting the cylinder and support system with a threaded bar. This threaded bar is used to position the cylinders in the acrylic glass, where the axial distance $\boldsymbol{L}$ of the cylinder's centers can be changed during the experiment. This configuration permits the lateral oscillatory movement of both cylinders. The flow passes only below the acrylic glass table, in a region with 1000 mm wide and 800 mm high. The cylinders are assembled so that 700 mm of their length is in contact with the flow.

The experiment was performed as follows: after properly assembling the setup, with a fixed $\boldsymbol{L/D}$ spacing ratio of interest, the axial blower was turned on with a specific rotational velocity. Once the airflow was stabilized, the acquiring system was turned on. When the data acquisition for this specific velocity was completed, the rotational velocity of the

axial blower was increased, and the data acquisition was turned on again. After testing all proposed flow velocities for this fixed $\boldsymbol{L/D}$ spacing ratio, the axial blower was turned off and a new $\boldsymbol{L/D}$ was assembled to repeat the same procedure.

The wake flow velocity was monitored using two hot-wire anemometers type DANTEC 55P11, designed with one wire perpendicular to the flow. These two hot wires were positioned in the wake of the downstream cylinder, 10 times the diameter far from the downstream cylinder's center. One anemometer was placed in the middle height of the downstream cylinder (Fig. 2b, detail B), and the other was placed parallel to the bottom tip of the cylinders (Fig. 2b, detail A). The lateral acceleration was measured by means of two accelerometers model ADXL335, inserted inside the circular cylinders and located in its bottom tip. This sensor is able to measure the acceleration in the $\boldsymbol{x}-$, $\boldsymbol{y}-$ and $\boldsymbol{z}-$axes, with a resonant frequency of 5.5 kHz and measurement range of ±3g. The anemometers were connected to the DANTEC StreamLine constant hot-wire anemometry system, and both accelerometry and anemometry data acquisition were taken by a 16-bit A/D board with a USB interface. The generated time series has 32,768 samples and a sampling frequency of 1000 Hz, which leads to a time series with 32.768 s. A low pass filter at 300 Hz was set to the anemometry data. The results were post-processed by the Matlab software applying statistical tools for the time domain, frequency domain, and time-frequency domain, using the Fourier and Wavelet analysis.

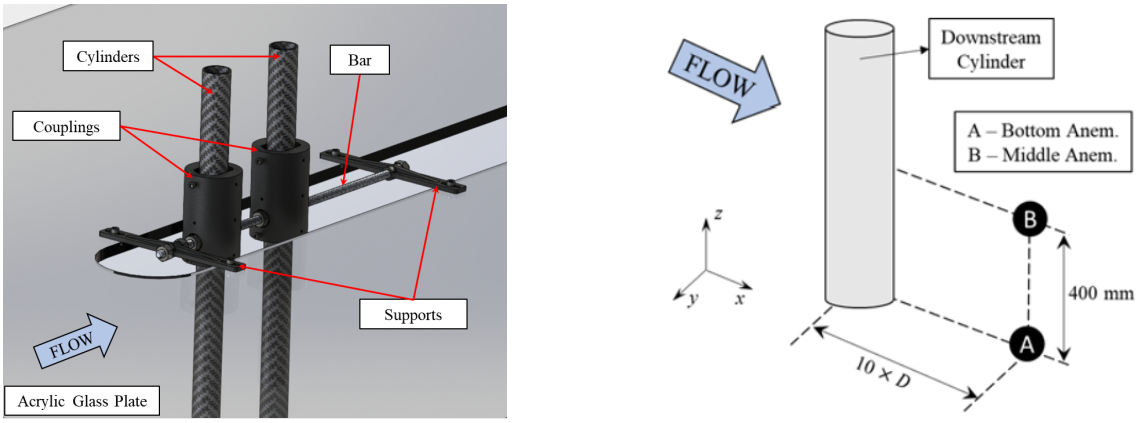

Figure 2 – Assembly of the cylinder's setup inside the wind tunnel (a), and details about the hot-wire anemometers behind the downstream cylinder (b).

The uncertainty in the velocity series results through the anemometry acquisition is in the range of 2–7%, while in the accelerometry acquisition, the uncertainty is ±1º. The uncertainty in the vortex shedding frequency values using the Fourier analysis depends on the bandwidth $\boldsymbol{Be}$ used and the average statistical error $\boldsymbol{\varepsilon}$. Typical values for these are about 2 Hz < $\boldsymbol{Be}$ < 4 Hz and 8% < $\boldsymbol{\varepsilon}$ < 13%, remaining at 1.90 Hz and 12.5% in the present work.

Two nondimensional relations in this study are relevant. These relations are the damping ratio ($\boldsymbol{\zeta}$), and the relation of the cylinder mass and the displaced air mass by the cylinder, called mass ratio ($\boldsymbol{m^*}$). For both upstream and downstream cylinders, the mass ratio is 216. The damping ratio of the cylinders was measured by the accelerometers with the logarithmic decrement technique. The values of the damping ratio for the upstream and the downstream cylinders are 0.0062 and 0.0046, respectively. Still, the natural frequency for each cylinder assembly is 46.88 Hz. Four free stream velocities of 5.7, 7, 9, and 10 m/s were proposed in this experiment, generating the Reynolds numbers of 9.5, 11.6, 15, and 16.6×10^3.

4. RESULTS

The acquired data was post-processed by the Matlab software applying the statistical tools previously mentioned. Firstly, the results of the accelerometers are presented, discussing the DWT results of the time series signal, statistical values, and predominant frequency. The second subsection presents the results of the velocity time series obtained from the hot-wire anemometers. DWT results, time domain statistical analysis, and energy content analysis are discussed.

4.1 Lateral acceleration results

Figure 3 presents the DWT analysis of the lateral acceleration time series, obtained from the accelerometers, for the highest Reynolds number of 16.6×10^3 and the $\boldsymbol{L/D}$ spacing ratios of 3, 4, and 5 (Fig. 3 a-c, respectively). It is clear that, for both upstream and downstream cylinders, the amplitude levels for spacing ratio $\boldsymbol{L/D}$ of 3 (Fig. 3a) are higher than the other proposed spacing ratios of 4 and 5 (Fig. 3 b and c, respectively). The higher the spacing ratio $\boldsymbol{L/D}$, the lesser the observed amplitude levels in Fig. 3.

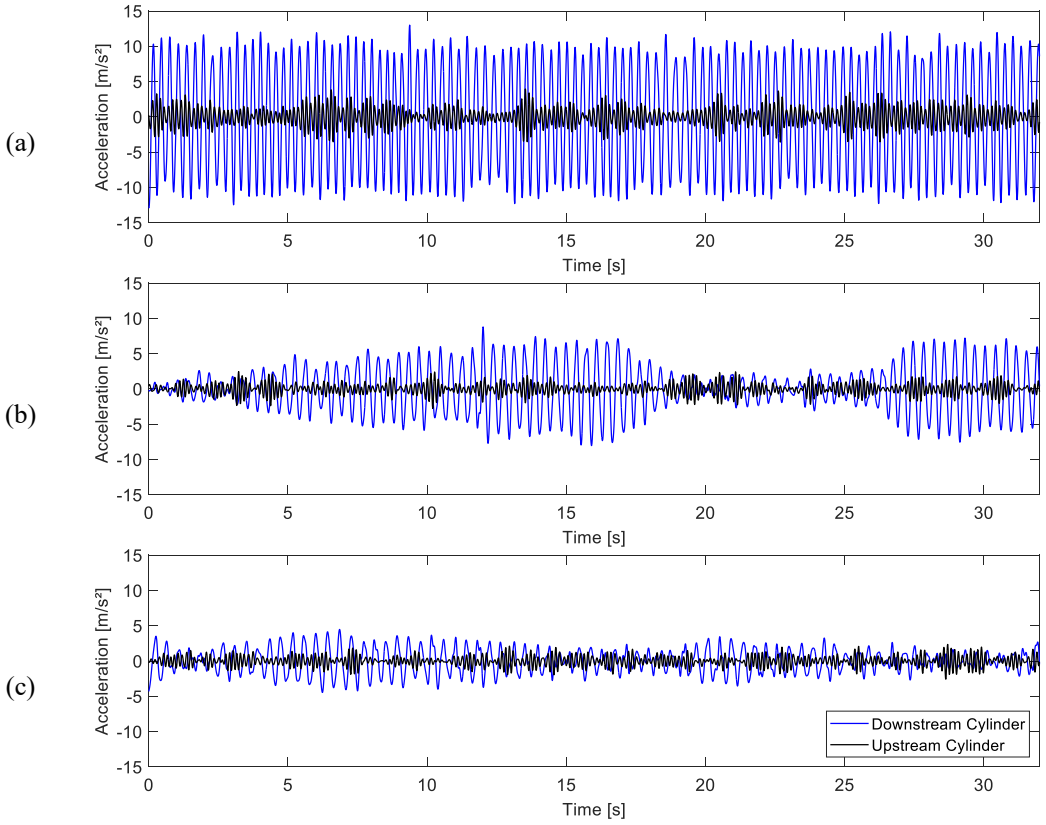

Figure 3 – DWT of acceleration results, $\boldsymbol{L/D}$ of 3, 4, and 5 (a–c, respectively), Re number of 16.6 × 10³.

The oscillation behavior and the amplitude levels of the upstream cylinder present very similar characteristics when the three proposed $\boldsymbol{L/D}$ spacing ratios are compared (black line of Fig. 3 a-c). On the other hand, when the same comparison is performed for the downstream cylinder, the highest amplitude levels are higher for the lesser spacing ratio, decreasing as the spacing ratio is increased. These results indicate that the upstream cylinder is less affected by the longitudinal distance than the downstream cylinder. When compared with other works with higher $\boldsymbol{L/D}$ spacing ratios of 8 and 10, this same behavior is also observed (Neumeister et al., 2022).

The results of Fig. 3 were statistically studied and extended to the other proposed Reynolds numbers by comparing the mean amplitude of the upstream and the downstream cylinders (MAUC and MADC, respectively). Also, a comparison of the fluctuation values observed in these results was performed by means of the standard deviation of the DWT acceleration signal. Figure 4 a-b and Fig. 5, respectively, present the mentioned analysis.

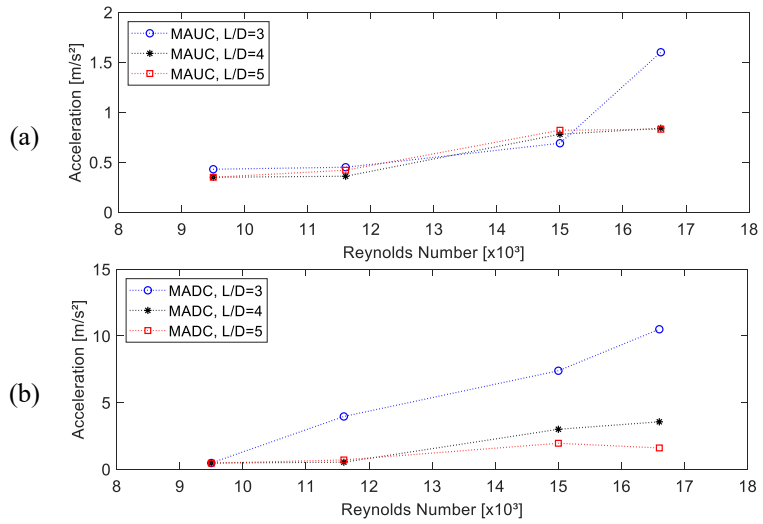

Figure 4 – Mean amplitude of the DWT signal of lateral acceleration for the upstream (a) and downstream (b) cylinders. MAUC – Mean Amplitude of the Upstream Cylinder, MADC – Mean Amplitude of the Downstream Cylinder.

For the upstream cylinder (Fig. 4a), the mean amplitudes of the lateral acceleration present a behavior almost linear, except for the spacing ratio of 3 and Reynolds number of 16.6 x 10^3, where a small increase in the amplitude was found. As the upstream cylinder is less affected by the $\boldsymbol{L}$ distance, this behavior was expected. Considering the downstream results (Fig. 4b), the spacing ratios of 4 and 5 present smaller values when compared with the spacing ratio of 3. The same "linear" tendency is observed, but the inclination of the line of the spacing ratio 3 is higher than the others. This increase of the amplitude in the acceleration results is very relevant considering energy generation applications.

To complement the above analysis, Fig. 5 presents the mean-time fluctuations in the lateral acceleration results of this study, where FAUC and FADC are the fluctuations in the lateral acceleration results of the upstream and downstream cylinder, respectively. For the smaller Reynolds number of 9.5 × 10^3, all the spacing ratios present practically the same results. Increasing the Reynolds number, the fluctuations values are proportionally increased. Although the results of the upstream cylinder increased, they still are smaller when compared with the downstream cylinder results. Emphasis for the $\boldsymbol{L/D}$ spacing ratio of 3 which presents the higher fluctuation values.

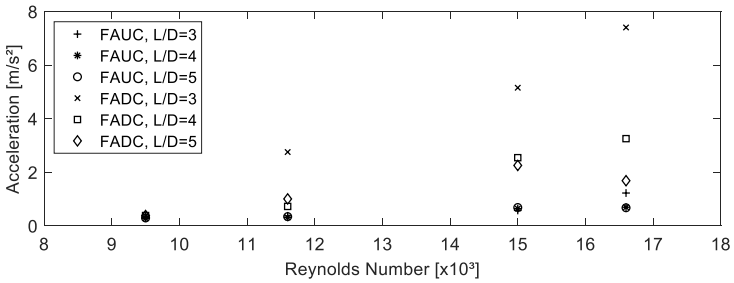

Figure 5 – Fluctuations in the DWT lateral acceleration results. FAUC – Fluctuations in the lateral Acceleration results, Upstream Cylinder, FADC – Fluctuations in the lateral Acceleration results, Downstream Cylinder.

4.2 Wake velocity results

The post-processed results of the wake velocity by means of the DWT analysis are presented in Fig. 6 a-c, for the proposed $\boldsymbol{L/D}$ spacing ratios of 3, 4, and 5, respectively, Reynolds number of 16.6 x 10^3, where the black line is the bottom anemometer results, and the blue line is the results of the middle anemometer (as detailed in Fig. 2b). The bottom probe presents values close to the imposed velocity of 10 m/s and very low fluctuation in its values. This behavior is observed in all the proposed $\boldsymbol{L/D}$ spacing ratios. One reason for this is the fact that the flow does not face any considerable obstacle in its path. In contrast, the wake flow velocity fluctuations observed in the middle of the cylinder present high values, since the wake in this region is very disturbed by the lateral movement of the downstream cylinder.

(a)

(b)

(c)

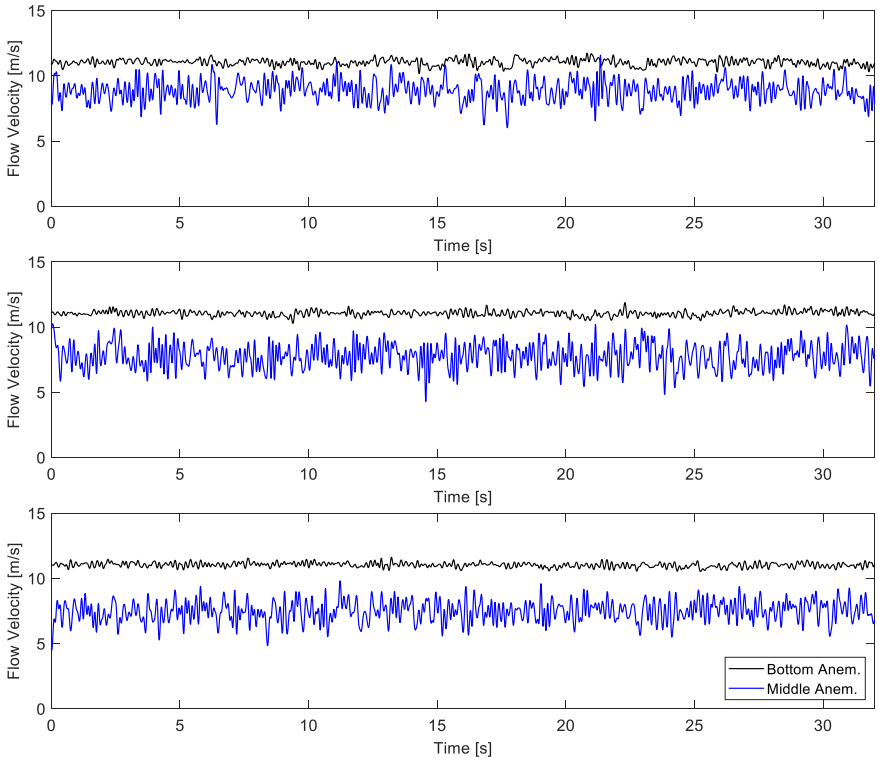

Figure 6 – DWT of wake velocity results, $\boldsymbol{L/D}$ of 3, 4, and 5 (a–c, respectively), Re number of 16.6 × 10^3.

Table 1 shows a time domain statistical analysis including the mean value (MV), the standard deviation (STD), the skewness (SK), and the kurtosis (K), of each result presented in Fig. 6 and also the other proposed Reynolds numbers. For the bottom anemometer, when comparing the same Reynolds number but varying the spacing ratio, the mean value of the wake velocity presents very similar values. In general, the same behavior is perceived for the standard deviation, skewness, and kurtosis of the upstream cylinder, considering only the bottom anemometer. It was already expected since the DWT time series of the bottom anemometer in Fig. 6 does not present high fluctuation levels and the signal is slightly symmetric.

On the other hand, considering only the middle anemometer and performing the same comparison, the mean values of the wake are very similar for the $\boldsymbol{L/D}$ spacing ratios of 4 and 5, and they are about 15% lesser than the mean values observed for the $\boldsymbol{L/D}$ spacing ratio of 3. The values of standard deviation, skewness, and kurtosis are very similar compared to the studied spacing ratios. Finally, comparing the overall results of the bottom and middle anemometers, the mean value of the bottom anemometers is higher than the middle anemometer, but the fluctuations and the signal asymmetry, measured by the standard deviation and the skewness, are higher for the middle anemometer. These results are a consequence of the already-mentioned characteristics of their positions. The kurtosis results are similar for both anemometers.

Table 1 – Time domain statistical results for all the proposed $\boldsymbol{L/D}$ spacing rations and Reynolds numbers. MV – Mean Value, STD – Standard Deviation, SK – Skewness, and K – Kurtosis.

		Bottom Anemometer				Middle Anemometer			
$\boldsymbol{L/D}$	Re [$\times 10^3$]	MV [m/s]	STD [m/s]	SK [m/s]	K [m/s]	MV [m/s]	STD [m/s]	SK [m/s]	K [m/s]
3	9.5	4.64	0.15	-0.04	2.59	3.76	0.58	-0.12	2.73
	11.6	7.07	0.18	0.00	3.02	5.64	0.67	-0.31	3.00
	15	9.26	0.22	-0.24	2.95	7.47	0.72	-0.34	3.03
	16.6	11.04	0.25	-0.28	2.94	8.86	0.76	-0.12	3.18
4	9.5	4.57	0.14	0.00	2.59	3.29	0.64	-0.06	2.58
	11.6	7.13	0.15	-0.02	3.19	4.81	0.77	0.04	2.64
	15	9.27	0.20	-0.15	2.76	6.45	0.85	-0.25	3.00
	16.6	11.06	0.20	-0.02	3.55	7.77	0.90	-0.06	2.80
5	9.5	4.68	0.16	-0.01	2.74	2.93	0.52	-0.11	3.06
	11.6	7.16	0.17	-0.14	3.04	4.62	0.67	-0.07	2.87
	15	9.11	0.23	-0.26	2.96	6.13	0.77	-0.14	3.03
	16.6	11.04	0.18	-0.07	2.83	7.49	0.76	-0.19	3.00

Two very pronounced peaks of ~ 48 Hz and ~250 Hz were found in the present study; the peak of ~ 48 Hz was found in the lateral acceleration results, while both peaks were observed in the wake velocity results. The first mentioned frequency represents the natural frequency of the system, while the second one indicates the physical mechanism involved in the flow interaction of the present investigation. The Strouhal number of ~ 0.21 was obtained by computing the results for the cylinder diameter $\boldsymbol{D}$, indicating the vortex shedding of the cylinders. The predominant frequency considering the lateral movement is about 2.4 Hz.

5. CONCLUSIONS

This article presented an experimental investigation where two circular cylinders free to oscillate in the lateral acceleration were tandem placed inside a wind tunnel. Three $\boldsymbol{L/D}$ spacing ratios varying the imposed flow velocity were tested, where $\boldsymbol{D}$ is the cylinder diameter and $\boldsymbol{L}$ is the longitudinal distance between the cylinder's centers, generating Reynolds numbers in the range of 9.6 to 16.6 × 10^3. The wake behind the downstream cylinder was monitored by the hot wire anemometer technique, located in the bottom and middle height of the downstream cylinder, while the lateral acceleration of both cylinders was measured by two accelerometers assembled inside the cylinders. The acquired data was post-processed using statistical analysis employing Fourier and wavelet analyses with the support of Matlab software.

Through the results presented in the lateral acceleration study, the $\boldsymbol{L/D}$ spacing ratio of 3 presented higher amplitudes when compared with the other proposed $\boldsymbol{L/D}$ spacing ratios, following the literature results. The upstream cylinder exhibited minimal sensitivity to the $\boldsymbol{L/D}$ spacing ratio, whereas the downstream cylinder displayed a significant dependence on this factor. The higher the $\boldsymbol{L/D}$ spacing ratio, the lesser the amplitude levels observed in the lateral acceleration results. Furthermore, the predominant frequency of the observed phenomenon is about 2.4 Hz.

Wake flow results emphasized the wake perturbation in the anemometer located at the middle height of the downstream cylinder due to its lateral movement. Statistical analysis indicated the high mean velocity of the flow located

in the bottom height of the assembly since this flow is not disturbed by the lateral movement of the cylinder, while wake flow fluctuations were observed in the other anemometer. Finally, two main frequencies were obtained in the energy content analysis, indicating the natural frequency of the system and the flow mechanism involved. Strouhal numbers computed to the cylinder diameter and the flow velocity identified the vortex shedding of the downstream cylinder.

Future works including the displaced lateral amplitude, more spacing ratios, and PIV technique are intended.

6. ACKNOWLEDGMENTS

This study was financed in part by the Coordenação de Aperfeiçoamento de Pessoal de Nível Superior - Brasil (CAPES) – Finance Code 001. This work had also partial financial support from the CNPq, Conselho Nacional de Desenvolvimento Científico e Tecnológico, Brazil, grant number 312133/2021-9.

7. REFERENCES

Alam, M. M. and Meyer, J. P., 2011. "Two interacting cylinders in cross flow". *Physical Review E - Statistical, Nonlinear, and Soft Matter Physics*, Vol. 84.

Alam, M. M., Moriya, M., and Sakamoto, H., 2003a. "Aerodynamic characteristics of two side-by-side circular cylinders and application of wavelet analysis on the switching phenomenon". *Journal of Fluids and Structures*, Vol. 18, p. 325–346.

Alam, M. M., Moriya, M., Takai, K., and Sakamoto, H., 2003b. "Fluctuating fluid forces acting on two circular cylinders in a tandem arrangement at a subcritical Reynolds number". *Journal of Wind Engineering and Industrial Aerodynamics*, Vol. 91, p. 139–154.

Assi, G.R.S, Bearman, P.W., and Meneghini, J.R., 2010. "On the wake-induced vibration of tandem circular cylinders: the vortex interaction excitation mechanism". *Journal of Fluid Mechanics*, Vol. 661, p. 365–401.

Chen, S. S., 1985. *Flow-induced vibration of circular cylindrical structures*. Washington, USA.

Chen, S. S., 1987. "A general theory for dynamic instability of tube arrays in crossflow". *Journal of Fluids and Structures*, Vol. 1, p. 35–53.

Derakhshandeh, J.F., Arjomandi, M., Dally, B., and Cazzolato, B., 2014. "The effect of the arrangement of two circular cylinders on the maximum efficiency of Vortex-Induced Vibration power using a Scale-Adaptive Simulation model". *Journal of Fluids and Structures*, Vol. 49, p. 654–666.

Habowski, P. B., de Paula, A. V., and Möller, S.V., 2020a. "Wake behavior analysis for two circular cylinders placed at several angles to the flow". *Journal of the Brazilian Society of Mechanical Sciences and Engineering*, Vol. 42, p. 441.

Habowski, P. B., Fiorot, G. H., de Paula, A. V., and Möller, S.V., 2020b. "Unbalanced free to oscillate tandem cylinders in a turbulent crossflow". In *Proceedings of ENCIT 2020, 18th Brazilian Congress of Thermal Sciences and Engineering*, Online.

Habowski, P. B., Neumeister, R. F, Petry, A. P., and Möller, S. V., 2022. "Numerical study of tandem slender cylinders on a turbulent crossflow". In *Proceedings of the 19th ENCIT – Brazilian Congress of Thermal Sciences and Engineering*, Bento Gonçalves, RS.

Indrusiak, M. L. S., Kozakevicius, A. J., and Möller, S. V., 2016. "Wavelet Analysis Considerations for Experimental Nonstationary Flow Phenomena". *Revista de Engenharia Térmica*, Vol. 15, p. 67.

Indrusiak, M. L. S., and Möller, S. V., 2011. "Wavelet analysis of unsteady flows: Application on the determination of the Strouhal number of the transient wake behind a single cylinder". *Experimental Thermal and Fluid Science*, Vol. 35, p. 319–327.

Igarashi, T., 1981. "Characteristics of the Flow around Two Circular Cylinders Arranged in Tandem: 1st Report". *Bulletin of JSME*, Vol. 24, p. 323–331.

Neumeister, R. F., Ost, A. P., Habowski, P. B., Paula, A. V. D., Petry, A. P., and Möller, S. V., 2022. "Wake induced vibration in tandem cylinders: Part 1 - Wake perturbation analysis". In *Proceedings of the 12th International Conference on Flow-Induced Vibration*, p. 103–110, Paris-Saclay, France.

Neumeister, R. F., Petry, A. P., and Möller, S. V., 2021. "Experimental Flow-Induced Vibration Analysis of the Crossflow Past a Single Cylinder and Pairs of Cylinders in Tandem and Side-by-Side". *Journal of Pressure Vessel Technology, Transactions of the ASME*, Vol. 143, p. 1–13.

Noufal, R., Alziadeh, M., and Mohany, A., 2022. "Control of vortex shedding and acoustic resonance of a circular cylinder in crossflow". In *Proceedings of the ASME Pressure Vessels & Piping Conference 2022*, Las Vegas, Nevada.

Païdoussis, M. P., 1982. "A review of flow-induced vibrations in reactors and reactor components". *Nuclear Engineering and Design*, Vol. 74, p. 31–60.

Park, C. Y., Lee, S. J., and Park, S. H., 2018. "Experimental investigation of vortex-and wake-induced vibrations of tandem cylinders". *Ships and Offshore Structures*, Vol. 13(8), p. 877-884.

Percival, D. B. and Walden, A. T., 2000. *Wavelet Methods for Time Series Analysis*. Cambridge University Press.

Priya, S., 2007. "Advances in energy harvesting using low profile piezoelectric transducers". *Journal of Electroceramics*, Vol. 19, p. 165–182.

Scarselli, G., Nicassio, F., Pinto, F., Ciampa, F., Iervolino, O., and Meo, M., 2016. "A novel bistable energy harvesting concept". *Smart Materials and Structures*, Vol. 25.

Sumner, D., 2010. "Two circular cylinders in cross-flow: A review". *Journal of Fluids and Structures*, Vol. 26, p. 849–899.

Tennekes, H. and Lumley, J. L., 1972. *A First Course in Turbulence*. The MIT Press.

Varela, D., Neumeister, R. F., Dias, G., de Paula, A. V., and Möller, S. V., 2017. "Experimental analysis of turbulent transversal flow on two fixed parallel cylinders with oscillatory and rotational freedom". In *Proceedings of the COBEM 2018 – 24th International Congress of Mechanical Engineering*, Curitiba, PR.

Zhou, Y., and Alam, M. M., 2016. "Wake of two interacting circular cylinders: A review". *International Journal of Heat and Fluid Flow*, Vol. 62, p. 510–537.

8. RESPONSIBILITY NOTICE

The authors are the only ones responsible for the printed material included in this paper.